



# Kinetics study of *ab*-plane crack propagation by a modulus measurement in single domain $\text{YBa}_2\text{Cu}_3\text{O}_x$

D. Shi <sup>a,\*</sup>, P. Odier <sup>b</sup>, A. Sulpice <sup>c</sup>, D. Isfort <sup>b,d</sup>, X. Chaud <sup>b,d</sup>,  
R. Tournier <sup>b,d</sup>, P. He <sup>a</sup>, R. Singh <sup>a</sup>

<sup>a</sup> *Department of Materials Science and Engineering, University of Cincinnati, Cincinnati, OH 45221-0012, USA*

<sup>b</sup> *Laboratoire de Cristallographie, CNRS, BP 166, F-38042 Grenoble Cedex 9, France*

<sup>c</sup> *Centre de Recherche sur les Très Basse Températures, CNRS, BP 166, F-38042 Grenoble Cedex 9, France*

<sup>d</sup> *CRETA, CNRS, BP 166, F-38042 Grenoble Cedex 9, France*

Received 12 March 2002; received in revised form 6 June 2002; accepted 14 June 2002

---

## Abstract

Young's modulus experiments have been carried out to study the kinetics of *ab*-plane crack propagation in single domain  $\text{YBa}_2\text{Cu}_3\text{O}_x$  (YBCO) during a prolonged oxygen heat treatment at 400 °C up to 188 h. It has been found that the modulus value experiences a rapid fall between the annealing time 48 and 96 h. X-ray diffraction (XRD) experiments have been carried out to investigate the structural phase transition during the oxygenation process. Consistently, a diffraction peak shift has been observed in this region that indicates a massive tetragonal-to-orthorhombic (T-to-O) transition. SQUID magnetization measurements of annealed samples have shown clear oxygen inhomogeneity in this regime suggesting a T-to-O phase boundary in the crystal. A physical model is provided to describe the operating mechanism of crack propagation in single domain YBCO.

© 2002 Elsevier Science B.V. All rights reserved.

*Keywords:* YBaCuO monodomain; Oxygenation; Tetragonal to orthorhombic transition; Crack propagation

---

## 1. Introduction

Growth of single domain  $\text{YBa}_2\text{Cu}_3\text{O}_x$  (YBCO) through peritectic reaction was long ago developed to produce large domains in which the weak links are significantly reduced in comparison to its sintered counterparts [1–11]. With controlled crystal orientation in the domain structure, it became

possible to achieve the desired superconducting properties in an appreciably large dimension of the superconductor for both fundamental studies and engineering applications. The importance of such progress lies in the industrial aspects of the research: a large domain structure allows engineering designers to consider many potential applications including magnetic levitation, long conductors, and microwave components while in polycrystalline materials, however, the glassy grain boundaries “smear” the sharpness of superconductivity leading to the weakly coupled nature of ceramic materials. In magnetic levitation, the lifting force is directly associated with the Meissner

---

\* Corresponding author. Address: University of Cambridge, Madingley Road, CB3 0HE Cambridge, UK. Tel.: +44-122-333-7073; fax: +44-122-333-7074.

E-mail address: [shid@email.uc.edu](mailto:shid@email.uc.edu) (D. Shi).

effect of a superconductor. Since the shielding currents are proportional to the domain size, research has been motivated towards making large domains for achieving even higher levitation force. Previous work has indicated that the levitation force is determined by the following factors: (1) domain dimension, (2) flux pinning strength, and (3) crystal orientation of the domain. Materials synthesis, specifically liquid-assisted processes have therefore focused on the growth of large domains with controlled crystal orientation and microstructure. A so-called seeded-melt-growth (SMG) method has been developed to produce such an ideal domain structure that offers optimum levitation capabilities.

As is well known, although the single domain structure has a single-crystal-like characteristic, there are small grain boundaries along *ab*-planes that can interfere with the superconducting current flow. Furthermore, the impurity phase  $\text{Y}_2\text{BaCuO}_5$  (2 1 1) is inevitably formed during the processing that is undesirable in some applications. Most importantly, cracks form during oxygenation due to the volume stress created during the phase transformation between tetragonal (T) and orthorhombic (O) structures. These cracks inherently exist in single domain YBCO that have been regarded as the most detrimental defect in the engineering applications. For instance, the mechanical strength of the YBCO is greatly reduced and the materials easily cleave along these *ab*-plane cracks. The levitation force or trapped field can also be severely limited due to these cracks. Therefore, extensive research has been carried out in the past in order to understand the crack formation and propagation mechanisms, and in turn to eliminate these *ab*-plane cracks. However, a few of these previous works focus on the kinetics of *ab*-plane crack propagation during oxygenation in single domain YBCO. In this study we have carried out modulus measurements on single domain YBCO samples that have been oxygenated for different times. Both X-ray diffraction and SQUID magnetization experiments have also been carried to determine the structure characteristics of phase transformation during the oxygenation. Kinetics of crack propagation has been studied based on these experimental results.

## 2. Experimental details

The SMG method was originally developed for the purpose of producing large domains for levitation applications [12–15]. In SMG, based on the concept of crystal growth, a small “seed” crystal of a higher melting point (compared to that of the precursor) is placed on the surface of the partially molten precursor material, and the initial growth can take place at the interface between the seed surface and the liquid during cooling. Furthermore, the growth assumes the orientation of the seed and eventually proceeds throughout the entire precursor material. In this way, a large single-crystal-like domain can be obtained in the sense that the whole material possesses only one crystal orientation.

In this growth experiment, the samples were disc shaped pellets (50 mm in diameter and 30 mm in height). We used precursors of 70 wt.%  $\text{YBa}_2\text{Cu}_3\text{O}_x$ , 30 wt.%  $\text{Y}_2\text{BaCuO}_5$ , and 0.15 wt.%  $\text{PtO}_2$ . These powders were thoroughly mixed and uniaxially pressed at 100 MPa into a disc shaped green pellet of 280 g. The green pellet was sintered in air at 930 °C for 24 h. A  $\text{SmBa}_2\text{Cu}_3\text{O}_x$  single domain was used as seed having a dimension of  $2 \times 2 \times 1.5 \text{ mm}^3$ . The seed was put on the top of the green pellet before the growth process. The green pellet was placed on an alumina plate with an intermediate layer of  $\text{Y}_2\text{O}_3$  powder to avoid liquid spreading on the interior surfaces of the furnace. A sintered thin plate of a mixture of  $\text{YbBa}_2\text{Cu}_3\text{O}_x$  and  $\text{YBa}_2\text{Cu}_3\text{O}_x$  was also used between the green pellet and the  $\text{Y}_2\text{O}_3$  layer. As will be explained later, this substrate was found necessary during the domain growth. After the completion of the domain growth, the sample was cooled in nitrogen gas to prevent the phase transformation from the tetragonal to orthorhombic structure. In this way, *ab*-plane crack formation is effectively suppressed. The details about the YBCO single domain growth can be found in Refs. [16–18].

A standard test method for dynamic Young's modulus for advanced ceramics was used to study the crack propagation by employing the Grindo Sonic MK5 “Industrial” instrument. This test method covers determination of the dynamic elas-

tic properties of advanced ceramics at ambient temperatures. Specimens of these materials possess specific mechanical resonant frequencies that are determined by the elastic modulus, mass, geometry of the test specimen. The dynamic elastic properties of materials can therefore be computed if the geometry, mass, and mechanical resonant frequencies of a suitable (rectangular or cylindrical geometry) test specimen of that material can be measured. Dynamic modulus is found using resonant vibrations. As microcracks form in the matrix of the YBCO, the vibration frequency will change sensitively leading to a reduced modulus of the materials. Therefore, the modulus measurement can be used as an effective tool to study the crack formation and propagation. In this experiment, YBCO bars of  $19 \times 5 \times 1.7 \text{ mm}^3$  were cut from the crack-free single domain pellet for the modulus experiment. The virgin sample had a tetragonal phase as it was cooled in nitrogen gas. The bar sample was annealed in flowing oxygen at  $400 \text{ }^\circ\text{C}$  between 8 and 188 h. At each annealing interval, the sample bar was cooled to room temperature and used for modulus measurement. After the modulus measurement, the sample was put back into the furnace for a prolonged oxygenation under the same condition up to 188 h. The flexure frequency was recorded at each annealing interval. The Young's modulus,  $E$ , can be therefore calculated based on the flexure frequency by the procedure below.

For the fundamental flexure frequency of a rectangular bar,

$$E = 0.9465(mF_f^2/b)(L^3/t^3)T_1$$

where  $E$  is the Young's modulus (Pa);  $m$  the mass of the bar (g);  $b$  the width of the bar (mm);  $L$  the length of the bar (mm);  $t$  the thickness of the bar (mm);  $F_f$  the fundamental resonant frequency of bar in flexure (Hz);  $T_1$  the correction factor for fundamental flexural mode to account for finite thickness of the bar

$$T_1 = 1 + 6.585(1 + 0.0752\mu + 0.8109\mu^2)(t/L)^2 - 0.868(t/L)^4$$

$$23 \left[ \frac{8.340(1 + 0.2023\mu + 2.173\mu^2)(t/L)^4}{1.000 + 6.338(1 + 0.1408\mu + 1.536\mu^2)(t/L)^2} \right]$$

$\mu$  is the Poisson's ratio;  $m = b \times t \times L \times d$ ;  $d$  the density of sample.

To analyze the oxygen content of the sample by SQUID magnetization and XRD measurement, small samples of  $5 \times 5 \times 1.7 \text{ mm}^3$  were also cut from the same single domain. Each of these small samples was placed in the furnace with the bar sample that was to be tested for modulus at each oxygen annealing interval. The samples used for magnetization and XRD were sectioned in the fashion depicted in Fig. 1. Note that the slice for XRD would indicate an averaged phase composition in the annealed sample. However, small rectangular rods were also cut from the similar slice for the magnetization SQUID measurements. Several such rods were cut from the same slice and measured to study the distribution of oxygenation for a given annealing time.

The powdered parts of the oxygenated samples were analyzed by X-ray diffraction (XRD) using a Siemens diffractometer (D5000) operating in transmission mode with the  $\text{CuK}\alpha$  radiation. The spectrum was recorded in the angular range  $10\text{--}100^\circ 2\theta$  and the lines of  $\text{YBa}_2\text{Cu}_3\text{O}_x$  phase (Y-123) indexed according to the Pmmm space group. Only the lines that do not overlap with those of  $\text{Y}_2\text{BaCuO}_5$  phase (2 1 1) were taken into account for calculation of the unit cell parameters by Cellref program. We then used 25 lines, which were sufficient to have an accurate indexing.

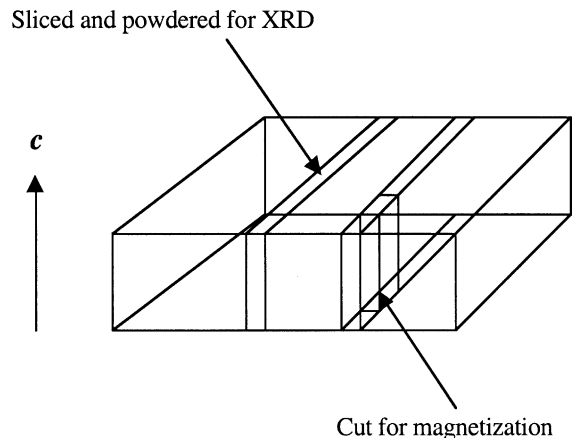


Fig. 1. Schematic diagram showing the section of YBCO samples for magnetization and XRD.

The magnetization measurement was carried out using a commercial SQUID magnetometer (Metronique Ingenierie) by applying the field along the  $c$ -axis. After cooling the sample in zero field, the magnetization was measured at 4.2 K up to 10 Oe in order to determine the susceptibility at low field for estimating the superconducting volume. At the same field the magnetization was measured in the zero-field cooled regime by heating the sample up to 95 K and the field cooled regime down to 4 K. The sample dimension was about  $1.7 \times 0.5 \times 0.5 \text{ mm}^3$ .

### 3. Results

Fig. 2a shows the microstructure of the as grown single domain YBCO. Due to flowing nitrogen during cooling, the YBCO phase remains un-oxygenated with a tetragonal structure. Lacking of volume stress induced by the T-to-O transition, no cracks are observed in this sample. However, as the sample was treated in flowing oxygen at 400 °C for 18 h, microcracks formed as

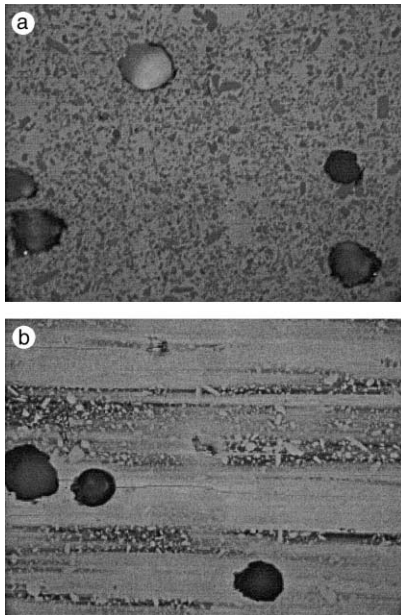


Fig. 2. Optical photographs showing (a) as grown, crack-free, and (b) oxygenated YBCO single domain sample.

shown in Fig. 2b, which have been typically seen in many previous studies. As the oxygen diffuses into the sample along the  $ab$ -planes, these microcracks also propagate into the interior of the domain structure at a rate that is comparable to that of oxygen diffusion. The propagation of the cracks is measured by the variation of the modulus as can be seen in Fig. 3. Fig. 3a shows the resonant frequency as a function of annealing time at 400 °C in flowing oxygen. Note in this figure, there are two similar samples oxygenated at the time for comparison. One of the samples starts with a high resonant frequency near 11 kHz when the an-

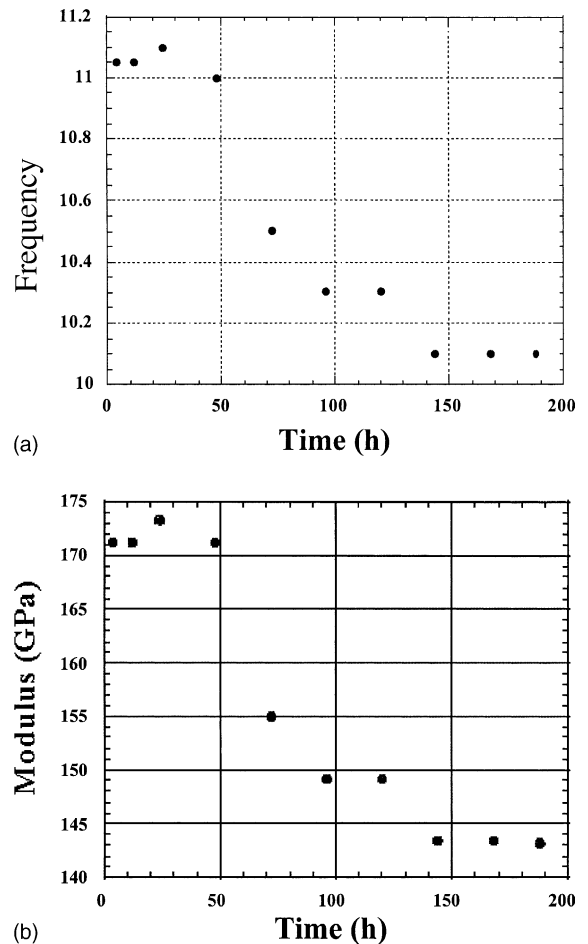


Fig. 3. Experimental results from modulus measurements: (a) resonance frequency versus annealing time, and (b) Young's modulus versus annealing time.

nealing time was set at 8 h. The frequency remains at more or less the same level up to 48 h, and thereafter begins to decrease in a quite pronounced fashion indicating the propagation of the micro-cracks. As the annealing time was prolonged to 96 h, the decrease in resonant frequency becomes much more gradual up to 188 h. A quite similar behavior can be seen from the other sample with the overall lower frequencies. Using the equations described in Section 2, we converted the resonant frequency values to Young's modulus. The data are shown in Fig. 3b. As expected, the modulus follows the exactly the same trend as a function of annealing time.

Fig. 4a shows the XRD spectra of all oxygen-annealed YBCO samples that have been measured for modulus. The spectra displayed in Fig. 4a show a significant amount of the 211 phase. Note that the volume percent of 211 changes from sample to sample suggesting a heterogeneous distribution of this phase. In Fig. 4b we focus on only the peaks near  $2\theta$  of  $23^\circ$ . As can be clearly seen, there is a peak shift between the annealing time of 48 and 60 h and this shift is completed at 92 h. The peak shift is a clear indication of T-to-O phase transition as has been extensively studied in the past. Based on these XRD data, we have calculated the  $a$ -,  $b$ -, and  $c$ -axis values that are plotted in Fig. 5. Clearly  $c$  and  $a$  (open symbol), behave similarly while  $b$  changes in the opposite. As a matter of fact the ratio  $c/a = 3.05$  remains constant while  $c$  shrinks of 1.2% and  $b$  elongates about 0.6%. As shown in Fig. 5a, both  $a$ - and  $c$ -axis experience a plateau region between 8 and 48 h. Thereafter, a sharp fall in  $a$  and  $c$  values is observed up to 92 h. These values remain more or less constant up to 188 h. The  $b$ -axis change is shown accordingly in Fig. 5b. Correspondingly,  $b$ -axis elongates as the annealing time increases. Again, the  $b$ -axis exhibits a constant between 8 and 60 h, then sharply takes off to its maximum at 120 h, and thereafter remains constant. The fall of  $c$ -axis occurs between 60 and 80 h of oxygenation and induces a severe stress possibly causing the opening of cracks in the  $ab$ -plane of the YBCO crystal.

As the T-to-O transition is mainly oxygen diffusion driven, it is important to determine the oxygen level of each annealed sample. In this study

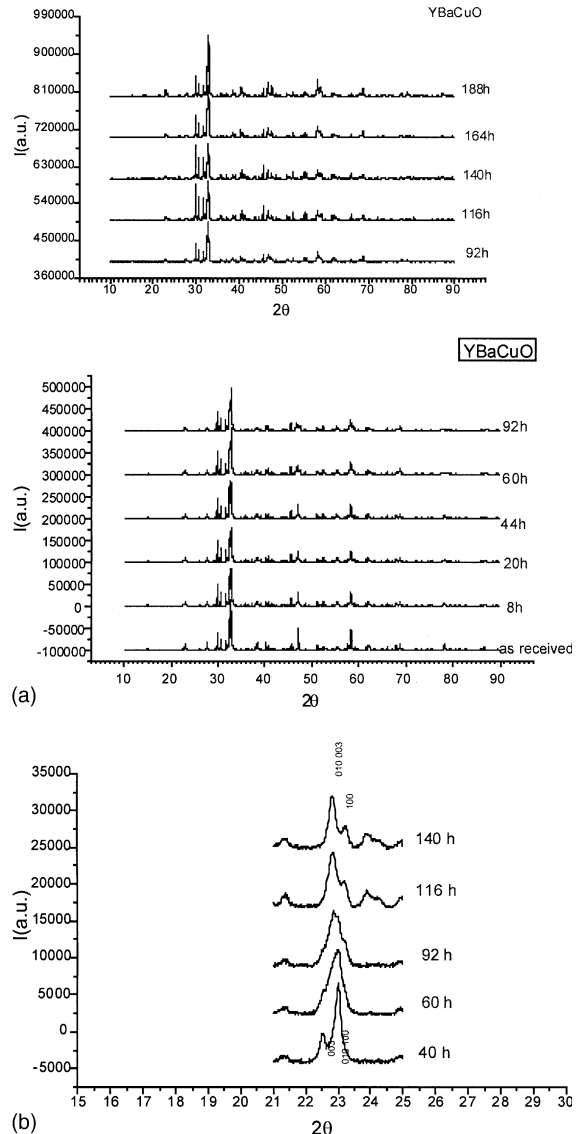


Fig. 4. (a) X-ray diffraction spectra of the sample annealed at the time indicated, (b) XRD data showing the peak shift.

we used SQUID-measured  $T_c$  as an indication of oxygen level. Fig. 6a shows the overall superconducting transitions of all samples annealed from 8 to 188 h. Clearly, the sample annealed up to 116 h all exhibit mixed phases as expected. This mixed phase indicates a T-to-O phase transformation front that may coincide with the propagating crack tips. Due to the inhomogeneous nature of the sample, we found that the  $T_c$  values differ

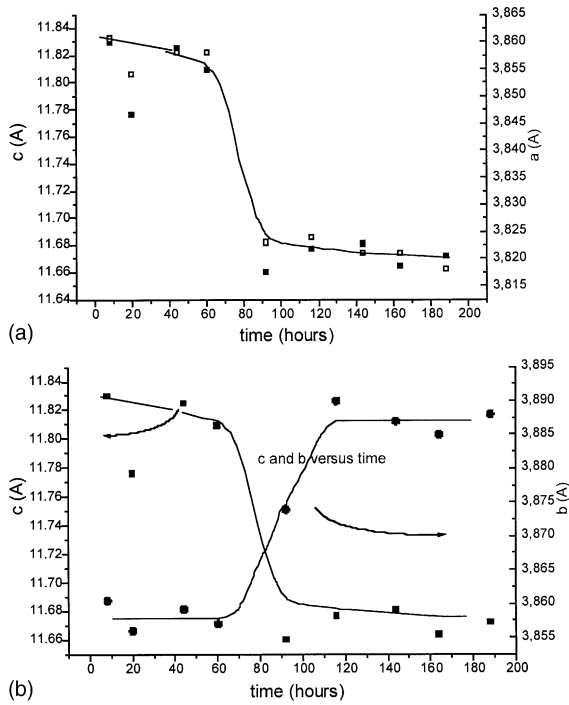


Fig. 5. Unit cell axis change as a function of annealing time: (a)  $c$  and  $a$  versus annealing time, and (b)  $b$  versus annealing time.

drastically even within the same sample. For instance, for the 68 h sample, three small separate pieces were cut from the bulk sample along the direction of oxygen diffusion. We have observed quite different superconducting transitions as indicated in Fig. 6b. Such inhomogeneity is the typical characteristic of the highly dense single domain YBCO. Therefore in Fig. 6a, some of the superconducting transitions may not be entirely consistent with each other, i.e., longer anneal may result in lower  $T_c$ 's due to this inhomogeneity.

The average volume percent of the superconducting phase can be determined by the slope of the Meissner effect. At low field, the measured susceptibility depends on the shape of the sample due to the influence of the demagnetizing factor. Therefore the precise calculation of the superconducting volume may be difficult as a result of geometry variation of the samples. Nonetheless, we may assume that the 188 h-annealed sample represents 100% of the superconducting volume. We have measured the magnetization,  $M$ , as a func-

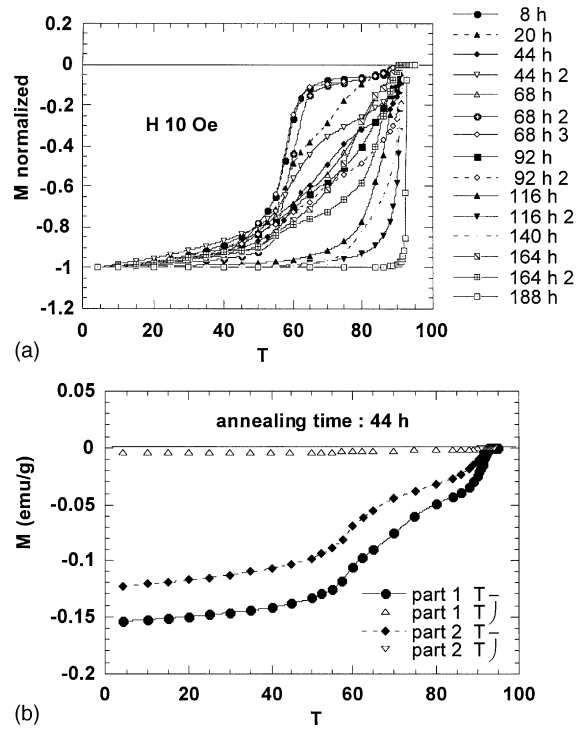


Fig. 6. (a) Magnetization versus temperature for the annealing time indicated, and (b) magnetization versus temperature for the sample annealed for 68 h.

tion of magnetic field,  $H$ , at 4.2 K at low field region, and results are shown in Fig. 7. The slope is proportional to the shielding current induced by the applied field, the stronger the shielding current

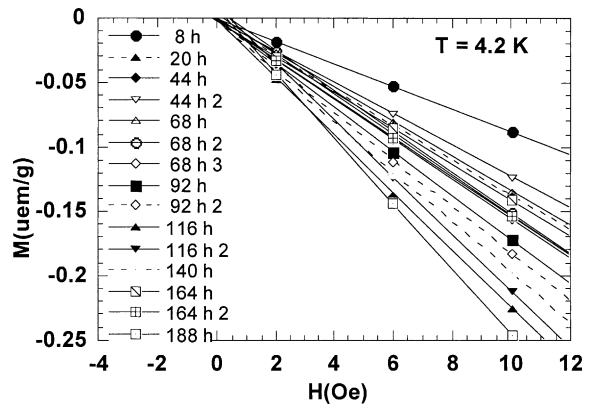


Fig. 7. Magnetization versus applied field at 4.2 K for the annealing temperature indicated.

the higher the volume percent of the superconducting phase which has the orthorhombic structure. Again, quite consistent with the behavior observed in Fig. 6a, the slope increases with oxygen annealing time up to 188 h, although inhomogeneity of oxygen has caused reversed effect in superconducting volume, i.e., longer annealed sample may have lower superconducting volume.

#### 4. Discussion

The YBCO system has been extensively studied in the past by means of various methods including neutron diffraction [19], X-ray diffraction [20] and transmission electron microscopy [21]. These experimental results have shown that the superconducting phase has an orthorhombic structure with space group Pmmm. The unit cell consists of  $\text{CuO}_2$  sheets in the  $ab$ -planes and  $\text{CuO}_3$  linear chains along the  $b$ -axis. The orthorhombic structure has been found to undergo an order–disorder transition at near 700 °C. The phase above 700 °C has been identified to have a closely related tetragonal structure which exhibits semiconducting behavior. The T-to-O phase transition is accompanied by an increase in oxygen occupancy along the  $b$ -axis between the Cu [1] atoms. As the total oxygen content of the sample is increased to above 6.5, the oxygen occupancy along both the  $b$ -direction is becoming higher than the  $a$  direction, leading to the T-to-O phase transition.

During the T-to-O transition both  $c$ - and  $a$ -axis will decrease, and accordingly the  $b$ -axis will increase as shown in Figs. 4 and 5. As a result of the variations along these axes there will be a volume change in the unit cell, in turn a large volume stress is produced. To accommodate such a large volume stress, the crystal would undergo twinning with their planes on the basal plane of the unit cell. For a polycrystalline YBCO or thin films the volume stress is sufficiently small and can be compensated due to their limited crystal dimensions. For a polycrystalline YBCO, the grain size is on the order of 50–100  $\mu\text{m}$ . The thin film would even have a smaller dimension on the order of 0.5  $\mu\text{m}$ . However, for a single domain YBCO the domain size can reach as large as 100 mm in diameter. The

volume stress produced during T-to-O transition can reach an extremely large value on the order of 1 GPa [22]. Such a high volume stress can deform the bulk single domain during the oxygen heat treatment. For a  $c$ -axis oriented single domain YBCO, the volume stress tends to shorten the crystal along the  $c$ -axis through out the  $ab$ -planes. As the single domain YBCO contains a high concentration of 211 particles, the  $c$ -axis change will be hindered by this isotropic second phase. As a result of 211 particles embedded in the matrix, the crystal deformation is inhomogeneous along the  $c$ -axis. Locally, the crystal tends to shrink along the  $c$ -direction elastically, however, the 211 particles stand as obstacles preventing the homogeneous deformation. As a result, the crystal cracks form along the  $ab$ -planes.

Suasmoro was the first to use the in situ ultrasonic wave attenuation to probe the microstructure of YBCO ceramics polycrystals [23]. He concluded, based on the ultrasonic data, that the microcracks formed in the tetragonal phase region where oxidation was taking place. Diko had made an extensive analysis on the behavior of microcracks in textured YBCO [24]. He elucidated on the origin of these cracks: i.e., whether these are growth defects or oxygen annealing defects. Growth defects were found parallel to the  $ab$ -planes due to a growth gap generated by inclusions of 211 particles during crystallization. Diko attributed the microcracking phenomena to a thermal expansion stress between oxidized and non-oxidized zones. The oxygenation was thought to be a combination of oxygen volume diffusion, microcracking, and oxygen penetration along the cracks.

Since the oxygen profile begins at the surface of the crystal, microcracks initiate there and propagate inward. The propagation velocity is related to the rate of oxygen diffusion. For a polycrystalline sample, the oxygen diffusion is quite rapid due to its short diffusion distance, taken as its grain size on the order of 50–100  $\mu\text{m}$ . In the previous studies by Shi et al., it was found that oxygenation was completed within 2 h in a 13 mm-diameter ceramic YBCO sample [25–27]. Oxygen diffusion in a single domain YBCO can be much slower due to its extremely high bulk density. The slow oxygen diffusion will dictate the kinetics of crack propagation

since the crack tip is likely at the diffusion front, or the interface region between the tetragonal and orthorhombic phases. Based on the experimental data of modulus shown in Fig. 3, we can see that the modulus value stays more or less the same up to 48 h of annealing time. The XRD results in Fig. 5 show that the *c*-axis also exhibits a plateau region. The magnetization experimental data in Fig. 6a indicate that the sample has a mixed phase at this annealing time. Further, in Fig. 7, we estimate that the volume percent of superconducting phase to be about 30 vol%. Therefore, the cracks formed are likely on the surface of the sample. These surface cracks have not effectively influenced the resonance frequency of the sample. Beyond the annealing time of 48 h, however, there is a rapid fall in resonance up to 96 h. Correspondingly, the XRD spectra in this region show a peak shift indicating a T-to-O phase transition as shown in Fig. 4b. Note that since XRD provides an average, bulk structural change, this peak shift implies the phase transition in a large volume percent in the sample. As shown in Fig. 5, the *c*- and *a*-axis also experience a pronounced change in this region. Such a massive phase transition should generate a large volume stress in the sample and cause the crack to propagate, which is reflected in the modulus change shown in Fig. 3. In this region, the sample is oxygen inhomogeneous with mixed T and O phases. We may then assume a T-to-O phase boundary where the cracks advance from the tetragonal region to the orthorhombic region as schematically depicted in Fig. 8. Thus, the oxygen inhomogeneity provides the driving force for crack propagation. Conder had given an exhaustive review of diffusion problems in YBCO by  $^{18}\text{O}$ – $^{16}\text{O}$  oxygen exchanges in polycrystals [28]. He clearly demonstrated that diffusion was faster in the chain direction parallel to the *ab*-planes. He also studied the kinetics of the low-temperature oxidation and showed that the oxidation diffusion kinetics was controlled by “a moving boundary” (interface between oxidized and non-oxidized zones) inside the grains. The rate of the boundary movement was constant with time and only temperature dependent. This picture is consistent with the physical model that we propose in this study.

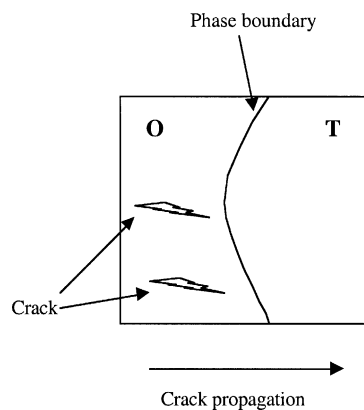


Fig. 8. Schematic diagram showing the phase boundary between the tetragonal and orthorhombic structures.

At annealing time around 100 h, as indicated by both XRD and the magnetization results, the sample is quite oxygen homogeneous although the superconducting transition is yet to be sharpened by further annealing. In an oxygen homogeneous sample, there is no T and O phase boundary, and the volume stress is significantly reduced. Lacking of driving force, the crack propagation slows down and eventually stops. Therefore, as shown in Fig. 2, the modulus value remains more or less unchanged up to 188 h.

Based on the experimental data from this study, we propose a physical explanation on the kinetics of crack propagation in single domain YBCO. In ceramics, tensile stress at the crack tip is required in order for the crack to propagate. In single domain YBCO, this stress is provided by the volume change during the T-to-O phase transition [29]. As the *c*-axis shortens, the 211 particles in the matrix remain elastically rigid and prevent the YBCO crystal to deform. In this way, *c*-axis tensile stress is produced in some localized region as schematically shown in Fig. 9, particularly near the 211 particles. As this tensile stress reaches the critical value, the microcracks are initiated on the surface. For these microcracks to propagate into the matrix of the domain structure, several conditions are required: (1) there must be an oxygen inhomogeneity in the sample matrix; (2) the sample must have an appreciable dimension in which enough volume stress can be generated; (3) an isotropic



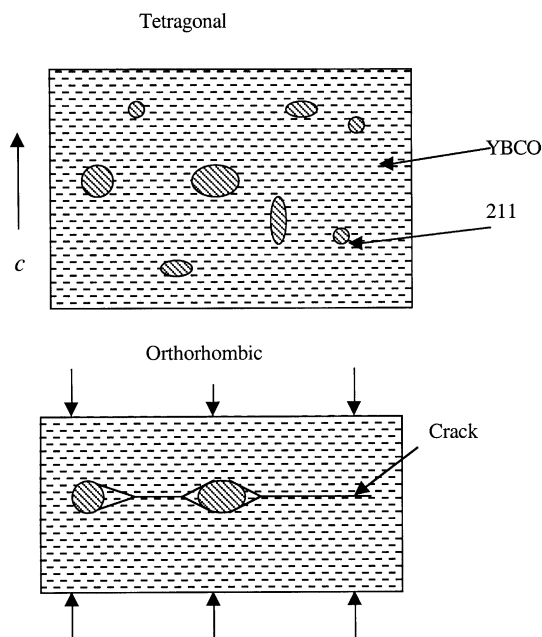


Fig. 9. Schematic diagram showing the tensile stress generated due to the combination of  $c$ -axis shrinkage and the rigid 211 particles in the crystal.

second phase should exist that can divert the compressive stress into tensile stress due to the  $c$ -axis shortening, and (4) a T-to-O phase boundary. As oxygen diffuses into the single domain, the profile establishes at the surface first where the oxygen level is the highest. As the oxygen reaches a value above 6.5, T-to-O phase transition takes place. At the low oxygen level in the orthorhombic structure, the volume stress created may be only moderate since the  $c$ -axis change is limited. Therefore the initial crack may form in the orthorhombic phase at some distance from the T-to-O phase boundary where the oxygen content is close to 6.5 (see Fig. 8). Further oxygen diffusion will advance the T-to-O boundary into the interior of the sample matrix. The crack tip follows this boundary movement; therefore the crack propagation is controlled by the rate of oxygen diffusion. As the oxygen level is homogeneously established in the sample, i.e. the T-to-O phase boundary eventually coincides in the domain matrix, the cracks have propagated throughout the entire crystal. No further cracks will be generated at the

surface; neither any crack propagation takes place in the interior of the crystal.

## 5. Conclusion

We have used Young's modulus measurement to study the kinetics of crack propagation in single domain YBCO. We have observed that the modulus value experiences a rapid fall in the annealing time period between 48 and 96 h. In this regime, based on XRD results, we have found a consistent peak shift that indicates a T-to-O phase transition. We conclude that this massive phase transition has created a large volume stress that is responsible for rapid crack propagation in the YBCO crystal. Due to severe contraction in the  $c$ -direction, the crystal undergoes a compressive deformation elastically. However the structurally isotropic 211 particles prevent the compressive deformation in some local areas especially near the 211 particles, therefore diverting the compressive stress to tensile stress. As the tensile stress reaches the critical value, the cracks begin to propagate inwardly in the crystal. The T-to-O phase boundary provides the driving force for the propagation of the cracks. Since the T-to-O transition is oxygen diffusion controlled, the kinetics of crack propagation is dictated by the rate of oxygen diffusion. After the oxygen content is homogeneously established in the sample, there is no further driving force for the propagation of the cracks.

## References

- [1] K. Salama, D.F. Lee, *Supercond. Sci. Technol.* 7 (1994) 177.
- [2] P.G. McGinn, W. Chen, N. Zhu, M. Lanagan, U. Balachandran, *Appl. Phys. Lett.* 57 (1990) 1455.
- [3] R.L. Meng, C. Kinalidis, Y.Y. Sun, *Nature* 345 (1990) 326.
- [4] J.C.L. Chow, W. Lo, C.D. Dewhurst, H.-T. Leung, D.A. Cardwell, Y.H. Shi, *Supercond. Sci. Technol.* 10 (1997) 435.
- [5] S. Jin, T.H. Tiefel, R.C. Sherwood, M.E. Davis, R.B. van Dover, G.W. Kammlott, R.A. Fastnacht, H.D. Keith, *Appl. Phys. Lett.* 52 (1988) 2074.
- [6] D. Shi, W. Zhong, U. Welp, S. Sengupta, V. Todt, G.W. Crabtree, S. Dorris, U. Balachandran, *IEEE Trans. Magn.* 5 (1994) 1627.

- [7] M. Murakami, M. Morita, N. Koyama, *Jpn. J. Appl. Phys.* 28 (1989) L1125.
- [8] V.R. Todt, S. Sengupta, D. Shi, J. Hull, P.R. Sahm, P.J. McGinn, R. Peoppel, *J. Electron. Mater.* 23 (1994) 1127.
- [9] D. Shi et al., *Physica C* 246 (1995) 253.
- [10] D. Shi, M. Xu, J.G. Chen, M.M. Fang, H. Krishnan, U. Welp, P.J. McGinn, W.H. Chen, M.T. Langan, K.C. Goretta, J.T. Dusek, J.J. Picciolo, J.M. Hong, D. Miller, U. Balachandran, *J. Appl. Phys.* 68 (1990) 228.
- [11] M. Cima, M. Flemings, A. Figueredo, M. Nakade, H. Ishii, H. Brody, J. Haggerty, *J. Appl. Phys.* 72 (1992) 179.
- [12] J.R. Hull, T.M. Mulcahy, K.L. Uherka, R.E. Erck, R.G. Abboud, *Appl. Supercond.* 2 (1994) 449–455.
- [13] K. Sawano, M. Morita, M. Tanaka, T. Sasaki, K. Kimura, S. Takebayashi, M. Kimura, K. Miyamoto, *Jpn. J. Appl. Phys.* 30 (1991) L1157.
- [14] M. Murakami et al., *Jpn. J. Appl. Phys.* 29L (1990) 1991.
- [15] K.Y. Blohowiak et al., *IEEE Trans. Appl. Supercond.* 3 (1993) 1049.
- [16] P. Gautier-Picard, X. Chaud, E. Beaugnon, A. Erraud, R. Tournier, *Mater. Sci. Eng. B* 53 (1998) 66.
- [17] D. Isfort, X. Chaud, E. Bourgault, R. Tournier, *Proceedings of EUCAS'99, Inst. Phys. Conf. Ser. No. 16* (2000) 47.
- [18] X. Chaud, D. Isfort, E. Beaugnon, R. Tournier, *Physica C* 341–348 (2000) 2413.
- [19] D. Jorgensen, *Jpn. J. Appl. Phys.* 26 (1987) 2017.
- [20] T. Siegrist, S. Sunshine, D.W. Murphy, R.J. Cava, S.M. Zahurak, *Phys. Rev.* 835 (1987) 7137.
- [21] J.G. Chen, D. Shi, C.M. Wayman, P.J. McGinn, W.H. Chen, N. Zhu, *Mater. Lett.* 14 (1992) 177.
- [22] D. Isfort, private communication.
- [23] Suasmoro, Ph.D. dissertation, 1992.
- [24] P. Diko, N. Pellerin, P. Odier, *Physica C* 247 (1995) 169–182.
- [25] D. Shi, D.W. Capone II, K.C. Goretta, K. Zhang, G.T. Goudey, *J. Appl. Phys.* 63 (1988) 5411.
- [26] D. Shi, K. Zhang, D.W. Capone II, *J. Appl. Phys.* 64 (1988) 1995.
- [27] D. Shi, *Phys. Rev. B* 39 (1989) 4299.
- [28] K. Conder, *Mat. Sci. Eng.* 32 (2001) 41–99.
- [29] P. Diko, *Mat. Sci. Eng.* 53 (1988) 149–153.